

Novel Group IVA (A) equiatomic hexagonal nitrides A_4N_4 (A = C, Si, Ge) with characteristic $\{A_2N_2\}$ layered tetrahedra: crystal chemistry and first-principles calculations

Samuel D. Griza, Samir F. Matar, Richard Wehrich, Volker Eyert

Angaben zur Veröffentlichung / Publication details:

Griza, Samuel D., Samir F. Matar, Richard Wehrich, and Volker Eyert. 2025. "Novel Group IVA (A) equiatomic hexagonal nitrides A_4N_4 (A = C, Si, Ge) with characteristic $\{A_2N_2\}$ layered tetrahedra: crystal chemistry and first-principles calculations." *Journal of Solid State Chemistry* 350: 125466. <https://doi.org/10.1016/j.jssc.2025.125466>.

Nutzungsbedingungen / Terms of use:

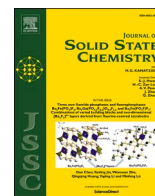
CC BY-NC-ND 4.0

Dieses Dokument wird unter folgenden Bedingungen zur Verfügung gestellt: / This document is made available under these conditions:

CC-BY-NC-ND 4.0: Creative Commons: Namensnennung - Nicht kommerziell - Keine Bearbeitung
Weitere Informationen finden Sie unter: / For more information see:

<https://creativecommons.org/licenses/by-nc-nd/4.0/deed.de>





Novel group IV^A (A) equiatomic hexagonal nitrides A₄N₄ (A = C, Si, Ge) with characteristic {A₂N₂} layered tetrahedra: Crystal chemistry and first-principles calculations

Samuel D. Griza^{a,*}, Samir F. Matar^b, Richard Wehrich^a, Volker Eyert^c

^a Institute of Materials Resource Management (MRM), University of Augsburg, Am Technologiezentrum 8, 86159, Augsburg, Germany

^b Lebanese German University (LGU), Sahel Alma, P.O.Box 206, Jounieh, Lebanon

^c Materials Design SARL, 42 Avenue Verdier, Montrouge, 92120, France

ARTICLE INFO

Keywords:

Carbonitrides
Lonsdaleite
DFT
Crystal structures
Mechanical properties
Phonon band structures

ABSTRACT

Superhard materials (Vickers hardness >40 GPa) are the key to demanding materials processing in industry scale and synthesis *via* high pressure routes like in diamond anvil cells. Despite extensive research both by experiments and computational chemistry, synthetic diamond (Vickers hardness $H_V \approx 90$ GPa) is still widely used. Sharing metastability and structure with diamond, softer cubic boron nitride cBN ($H_V \approx 60$ GPa) found application as e.g. refractory material where diamond lacks chemical resistance. This is most prominent in contact with iron containing compounds, ruling out diamond-coated machining tools for steels. While there are improvements of those materials like grain and grain boundary optimizations, none has reached wider industrial application due to processing difficulty and costs. Based on the tetragonal coordination of diamond and cBN, the present work addresses the question of novel superhard materials from the class of carbonitrides C_xN_y and its analogues from Group IV^A. A novel family of hexagonal A₄N₄ structures with A = C, Si, Ge is proposed based on crystal chemistry considerations and structure optimizations using Density Functional Theory with the Generalized Gradient Approximation. The structures are characterized by {A₂N₂} bilayers of AN polyhedra separated by repulsive N–N interactions. Due to short covalent bonds, the carbonitride is predicted to classify as superhard material. *Ab initio* calculations indicate thermodynamically and dynamically stable C₄N₄ at ambient conditions, laying the foundation for successful synthesis at $p > 40$ GPa in the future.

1. Introduction

The carbonitrides C_xN_y are considered as candidate ultra-hard materials challenging diamond (Vickers hardness $H_V \approx 90$ GPa [1]) for applications in deposition layers since long, as the prediction of shorter bond lengths than in diamond is a criterion for selecting this class of materials [2–5]. In particular, the theoretically proposed nitrogen-rich C₃N₄ has been in the focus since the mid-1990s as chemical analogue to existing Si₃N₄ [6]. However, the actual existence of such nitrogen-rich carbonitrides (N/C > 1) was long questioned due to the high nitrogen content that could not be achieved in syntheses by deposition methods. At the atomic scale, the repulsion energy from free electron pairs of N atoms turned out as one reason for the instability of these structures according to electronic localization calculations. On the carbon-rich side, sub-nitrides like C₇N₄, C₁₁N₄ were proposed with ultra-hard

mechanical properties and as models for spectroscopic characterizations of carbonitrides [7]. Mixed compounds like BC₂N, SiC₂N₄ or Si₂CN₄ that avoid short contacts of free electron pairs from N atoms were proposed by density functional theory and found experimentally (see, e.g., Refs. [8–10]).

CN₂ was found to be preferred in a corrugated layered structure as γ -CN₂. Many attempts to synthesize C₃N₄ started from precursors like C₂N₂(NH), that is close to equiatomic, synthesized by E. Horvath-Bordon et al. [11] and further analysed [12]. C₃N₄, originally discovered by J. J. Berzelius and named by J. von Liebig [13], rose to prominent interest in photochemistry [14].

At equiatomic 1:1 composition, ‘CN’ is known as gaseous cyanogen in form of N \equiv C–C \equiv N linear molecules (dicyan). Cyanogen was first described by Gay-Lussac in 1816 from HCN, ClCN, and Hg(CN)₂, probably earlier by Scheele in 1782 [15]. In 1847, Delbrück reported on the

* Corresponding author.

E-mail addresses: samuel.griza@uni-a.de, samuel.griza@pm.me (S.D. Griza).

<https://doi.org/10.1016/j.jssc.2025.125466>

Received 25 February 2025; Received in revised form 6 May 2025; Accepted 2 June 2025

Available online 4 June 2025

0022-4596/© 2025 The Authors. Published by Elsevier Inc. This is an open access article under the CC BY-NC-ND license (<http://creativecommons.org/licenses/by-nc-nd/4.0/>).

polymerization of cyan to paracyan [16]. F. Wöhler described solid CN, however, no chemical structures were known from experiment. In the solid state, a zero-dimensional orthorhombic crystal structure was proposed with arrangements of isolated $\text{N} \equiv \text{C}-\text{C} \equiv \text{N}$ linear molecules with bond length of 1.17 Å indicating a triple bond [17]. In a recent review reporting theoretical investigations on the C–N phase diagram, equiatomic CN was identified in tetragonal forms at high pressures using the *ab initio* evolutionary algorithm USPEX [18]. A comprehensive overview on predicted and synthesized carbonitrides was given by E. Kroke and M. Schwarz [19]. There is one breakthrough regarding synthesis of stoichiometric CN compounds: Stavrou et al. reported a route by the elements at 55 GPa and 7000 K, resulting in orthorhombic β -InS structure with a 3D network of sp^3 C–C and C–N bonds, but this compound decomposed below 6 GPa external pressure [20].

Extending to the analogues within group 14, ‘SiN’ and ‘GeN’ are not described, yet in the related series, Si_3N_4 as well as Ge_3N_4 are known in different modifications (further reading in, e.g., Refs. [21–25]). As we predicted pyrite type AN_2 ($A = \text{C}, \text{Si}, \text{Ge}$) 20 years ago [26], GeN_2 [27] and SiN_2 [28] were prepared by experiment in recent years. These pyrite-type structures show N–N dumbbell motives avoiding N lone electron pairs.

The lack of layered solid ‘AN’ with $A = \text{C}, \text{Si}, \text{Ge}$ stable at ambient conditions serves as a starting point of the present work which investigates the novel equiatomic hexagonal $(\text{CN})_4 = \text{C}_4\text{N}_4$ system. It is proposed with characteristic $\{\text{C}_2\text{N}_2\}$ bilayers of tetrahedra as a potential candidate. The extension to $A = \text{Si}$ and Ge addresses the effect of the A atom on the stability of AN compounds like our earlier investigations on AN_2 compositions.

The article is organized as follows: First, the novel structural model is derived on expansion of the lonsdaleite structure. This model was optimized to a relaxed ground state, before mechanical and electronic properties were calculated, i.e., elastic tensor, hardness, brittleness, electronic band structure, density of states, localization of electrons, phonon dispersions, and thermodynamic functions.

1.1. Computational methodology

This study employs quantum mechanical calculations within the framework of density functional theory (DFT) [29,30]. Structure optimizations as well as calculations of the mechanical and dynamical properties were carried out using the Vienna Ab initio Simulation Package version 6.3.2 (VASP6) [31,32] as implemented in *MedeA* 3.6.3 software of Materials Design together with projector augmented wave (PAW) potentials [33] and a plane-wave cutoff of 400 eV. Exchange and correlation effects were considered within the generalized gradient approximation (GGA) as proposed by Perdew, Burke, and Ernzerhof (PBE) [34] with corresponding PAWs PBE N (April 8, 2002), PBE C (April 8, 2002), PBE Si (January 5, 2001) and PBE Ge (January 5, 2001). While PBE and other gradient corrected functionals rely on a semi-local approach to electronic exchange and correlation, van der Waals forces are addressed within Grimme’s empirical correction term DFT-2D to the standard GGA DFT detailed elsewhere [35]. Brillouin-zone integrals were calculated using the tetrahedron method with Blöchl corrections [36] and a Monkhorst-Pack \vec{k} -point mesh with $6 \times 6 \times 4$ to $12 \times 12 \times 8$ points [37]. The structural optimizations were performed using the conjugate gradient method until the atomic forces were below $0.02 \text{ eV}/\text{Å}$ and all stress components were less than $0.003 \text{ eV}/\text{Å}^3$. Charge transfer trends were analysed by the atoms-in-molecules approach introduced by Bader [38]. Applying Bader analysis results in atomic basins according to the definition of zero-flux-surfaces. These can be understood as points between atoms where sample electrons are attracted similarly by neighboring atomic cores. Integrating the electronic density within the basins results in numbers of electrons n_e that allow for the calculation of atomic charges $n_{\text{ch}} = Z - n_e$. For AX compositions the charge is similar the charge transfer from atom A to X with

$\delta = n_{\text{ch}}$. Properties related to electron localization were obtained from a real-space analysis of the electron localization function according to Becke and Edgecomb [39], which was initially devised for Hartree–Fock calculations and later adapted to DFT methods and which is based on the kinetic energy density with the Pauli exclusion principle considered. The resulting function *ELF* is normalized ($0 < \text{ELF} < 1$) with 3D projections and plane slices usually explicated in the form of color maps. Computation of mechanical properties was performed with the *MedeA* MT module employing symmetry-general least-square extraction of elastic coefficients described by LePage and Saxe [40,41]. Brillouin-zone scanning of phonons was done according to Togo et al. [42] within integrated PHONON Software 6.14 by Parlinski [43]. Topology analysis was performed with TopCryst online tool [44] based on the Topological Types Database. Energies of formation were calculated with optional external pressure comparing the VASP total energies of an A_4N_4 unit cell $E_{\text{A}_4\text{N}_4}^{\text{UC}}$ and of the respective most stable modification of the elements at $T = 0 \text{ K}$, E_A^{atomic} . This can be expressed as $E_{\text{formation}} = E_{\text{A}_4\text{N}_4}^{\text{UC}} - 4E_A^{\text{atomic}} - 4E_{\text{N}}^{\text{atomic}}$, because 4 + 4 atoms constitute the unit cell. The considered modifications are for carbon *P6₃/mmc* graphite [45] and *Fd-3m* diamond [46]; for silicon *Fd-3m* [47], *I4₁/amd* [48], *P6/mmm* [49], *P6₃/mmc* [50] and *Fm-3m* [51] according to Li et al. [52]; for germanium *Fd-3m* [53], *I4₁/amd* [54]; and for nitrogen *Pa-3* crystal [55,56]. Complementary calculations are performed with the metaGGA functionals revTPSS by Tao et al. [57,58] and *r*²SCAN by Furness et al. [59]. MetaGGA includes contributions of the kinetic energy density. Therefore, it is considered as a step further on Perdew’s Jacobs Ladder of density functional approximations [60]. Lastly, unit cells and crystal structure motives were plotted in Diamond 4.6.8 software of Crystal Impact.

2. Results and discussion

2.1. Structure characterisation and crystal chemistry

To build layered AX compounds in contrast to CsCl-, NaCl- or ZnS-type coordinations, knowledge from C_3N_4 on decreased stability of C–N, C–C and N–N single bonds is applied. Starting from lonsdaleite

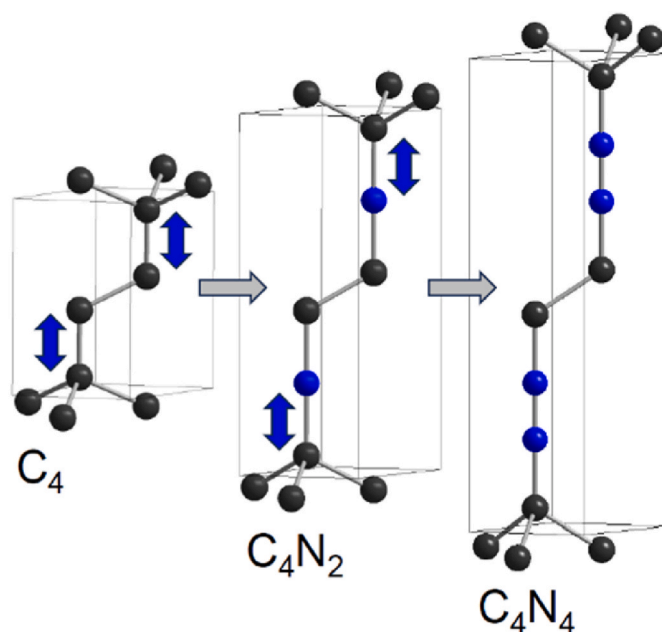


Fig. 1. Expansion of hexagonal lonsdaleite C_4 (left) by adding one nitrogen atom to (middle) C_4N_2 and two nitrogen atoms to form the proposed C_4N_4 (right). Carbon atoms in black, nitrogen in blue. (For interpretation of the references to color in this figure legend, the reader is referred to the Web version of this article.)

structure C_4 , i.e., hexagonal diamond with space group $P6_3/mmc$ (No. 194), as shown in Fig. 1 on the left with four carbon atoms per unit cell ($Z = 4$) at $4f$ position ($2/3 \mid 1/3 \mid z$) - cf. the middle structure - with $z \approx 0.95$. Inserting N at the $2c$ position ($2/3, 1/3, 3/4$) like in the middle structure leads to an increase of the hexagonal c -axis. The resulting C_4N_2 system was submitted to unconstrained geometry optimization and found energetically stable with the same space group as lonsdaleite. The investigation of this carbonitride revealed dynamic instabilities as indicated by imaginary acoustic phonons modes. Introduction of additional nitrogen led to four N atoms per unit cell at the $4f$ position ($2/3, 1/3, z$) with C_4N_4 stoichiometry as shown in Fig. 1 on the right-hand side. In principle, this structure allows for the formation of N–N bonds related to our earlier investigated AN_2 models. However, DFT relaxation to the ground state yielded a bilayer structure of tetrahedra. The atomic distance is determined as $d(C-N) = 1.455 \text{ \AA}$, which is typical for strong C–N single bonds. N–N distances of 2.632 \AA (intra-layer) and 2.975 \AA (inter-layer) do not indicate N–N bonding but formation of free electron pairs and N atoms with a tendency to repulsion and structuring of layers. Closer investigation pointed to a major role played by the $N(2s^2)$ lone pair in the formation of the new structure as discussed below in the context of electron localization. There is a deviation from the ideal tetrahedral angle of 109.47° especially in the case of C_4N_4 . The relaxed crystal structures are presented in Fig. 2 with relevant parameters summarized in Table 1. C_4N_4 and Si_4N_4 can be characterized with $3,4L147$ topology, while Ge_4N_4 obeys a honeycomb structure with hcb topology. Subsequent literature search showed that such topology characterizes layered chalcogenides as GaS [61] and InSe [62].

Energies of formation of the proposed structures were found to be $+2.44 \text{ eV}$ (C_4N_4), -6.57 eV (Si_4N_4) and $+0.43 \text{ eV}$ (Ge_4N_4) per unit cell, i.e., Si_4N_4 is found thermodynamically stable at ambient pressure. For comparison, the energy of formation of the tetragonal structure of CN mentioned by Dong et al. [18] was calculated and found to have the same magnitude as that obtained for C_4N_4 . Though the carbon nitride is predicted metastable with respect to the educts at ambient pressure, this changes above $p_{\text{external}} = 40 \text{ GPa}$ similar to PtN_2 [63]. The pressure dependency is depicted up to 400 GPa in Fig. 3 based on results in appendix Table A2. This indicates that these structures might be accessible as metastable compounds at high pressure similar to diamond, lonsdaleite, PtN_2 or phosphorous [64].

2.2. Electronic properties

Fig. 4 shows the projected charge densities exhibited as red regions centered at the N atoms of the three calculated A_4N_4 structure. The calculated values of charge transfer δ are: $\delta(C_4N_4) = \pm 0.9019$, $\delta(Si_4N_4) = \pm 2.2345$ and $\delta(Ge_4N_4) = \pm 1.3525$, all occurring from A (C, Si, Ge) to N and indicating a decrease of covalence from C to Ge and then to Si. These results follow the same trend as CN_2 , SiN_2 and GeN_2 [26].

Indeed, the respective Pauling electronegativities χ of the atomic

Table 1

Crystal structure parameters from GGA with PBE + D2. Note that the formation energy of lonsdaleite (hexagonal diamond) is -2.4 eV/atom .

| $P 6_3/m m c$ (Nr. 194) | C_4N_4 | Si_4N_4 | Ge_4N_4 |
|---|--|---|---|
| a in \AA | 2.3634 | 2.8844 | 3.0881 |
| c in \AA | 10.5630 | 12.2023 | 12.3956 |
| V_{cell} in \AA^3 | 51.10 | 87.91 | 102.38 |
| V/atom in \AA^3 | 6.39 | 10.99 | 12.80 |
| Shortest distance in \AA | 1.455 (C–N) | 1.752 (Si–N) | 1.893 (Ge–N) |
| Angles | N–C–C: 110.3° N–C–N: 108.6° | N–Si–Si: 108.1° N–Si–N: 110.8° | N–Ge–Ge: 109.6° N–Ge–N: 109.3° |
| Atomic position, $4f$ ($2/3, 1/3, z$) | $z(C) = 0.1732$ $z(N) = 0.8746$ | $z(Si) = 0.1521$ $z(N) = 0.8925$ | $z(Ge) = 0.1492$ $z(N) = 0.9022$ |
| E_{tot} in eV | -67.88 | -62.08 | -51.73 |
| $E_{\text{formation}}$ per UC in eV | $+2.44$ | -6.57 | $+0.43$ |

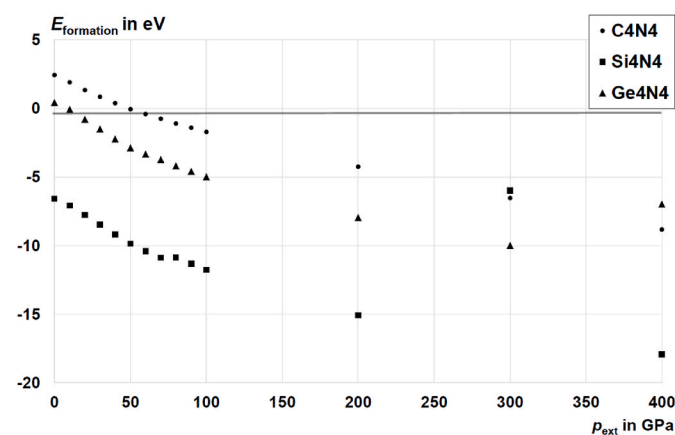


Fig. 3. Pressure dependence of formation energy of A_4N_4 based on data presented in appendix Table A2. Negative values indicate a thermodynamically stable compound at the respective external pressure.

constituents reflect these observations: $\chi_C = 2.55$, $\chi_{Si} = 1.90$, $\chi_{Ge} = 2.01$ versus $\chi_N = 3.04$, leading to $\Delta\chi_{C-N} = -0.49$, $\Delta\chi_{Si-N} = -1.14$, and $\Delta\chi_{Ge-N} = -1.03$.

The arrangement of the structures in terms of 2D-like corner sharing tetrahedra instead of a 3D arrangement can be assessed from the projection of the electron localization function ELF . The left of Fig. 5 shows the diagonal ELF plane of A_4N_4 with blue (0) for no localization, green (1/2) for free-electron-like localization and red (1) for full localization. The characteristic bilayered tetrahedral arrangements can be identified from the blue areas surrounding the two $\{A_2N_2\}$ blocks in the three

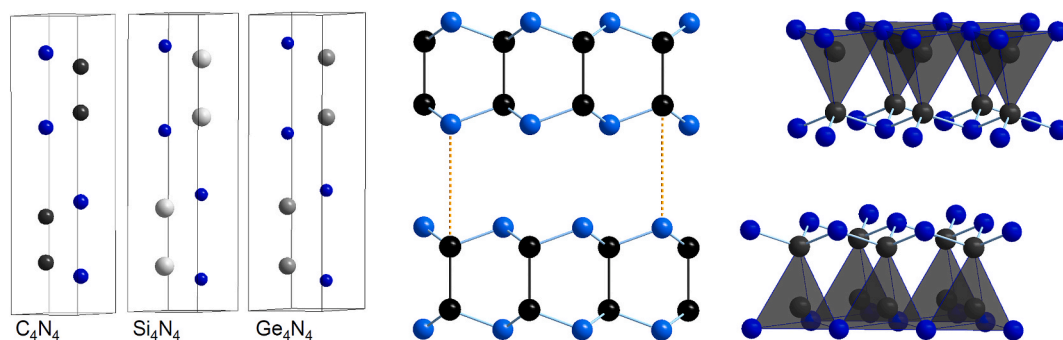


Fig. 2. Relaxed unit cells with nitrogen in blue, carbon in black, silicon in silver, germanium in anthrazite (left). Layered structure with bonds and dashed orange lines parallel to z -axis to indicate layer stacking (middle). Edge connected A_4N_4 tetrahedra with additional connecting nitrogen atoms forming bilayers (right). (For interpretation of the references to color in this figure legend, the reader is referred to the Web version of this article.)

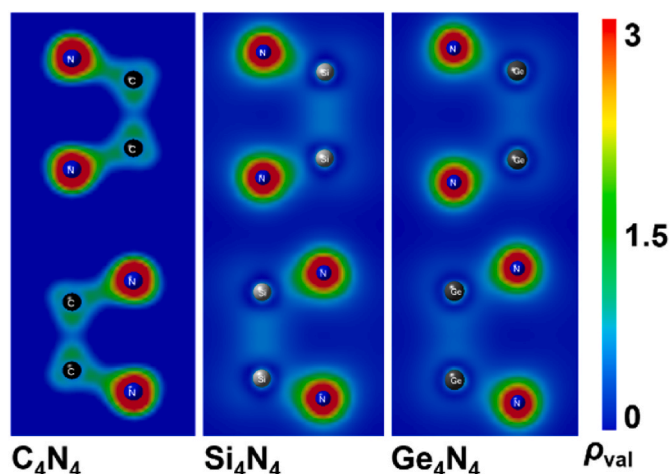


Fig. 4. Projection of valence charge densities along the long diagonal of the unit cells. While the surrounding charge density at nitrogen atoms (blue) stays similar, the character changes from carbon to germanium towards less density at the A atoms and more diffuseness of the respective A-A bonds. (For interpretation of the references to color in this figure legend, the reader is referred to the Web version of this article.)

chemical systems separated by a large distance of ~ 3 Å. To the opposite, within the blocks the red areas between the atoms indicate bonding between the different atoms, *i.e.*, A-A and A-N, which increase across the series. The right side of Fig. 5 depicts the relevant feature of large localization at N exhibited besides the bonding with A, *i.e.*, the non-engaged or non-bonded large ELF envelopes (red) pointing in the vertical direction (*c*-hexagonal axis) with the largest volume in C_4N_4 corresponding to $N(2s^2)$. Such interatomic lone-pair interaction is proposed to play a major role in the structuring of A_4N_4 . This effect can be assessed on different levels: First, non-bonding electrons influence van der Waals and pressure effects by demanding space in the unit cell. In the proposed structure, this leads to nitrogen atoms with similar coordination to NH_3 , where the lone pair *E* can be treated like a bonding partner in the context of resulting $[NH_3E]$ polyhedra. Furthermore, in a layered arrangement lone-pair electrons determine both the layer equilibrium distance and attractive forces between them. For in depth description, *e.g.* Galy and Matar studied AsF_3 as a compound where lone-paired electrons at all atoms lead to isolated triangular pyramids [65,66]. Furthermore, a previous ab-initio study on experimentally found monoclinic Se_2TiO_6 could clearly show that lone-pair electrons are fundamental for this

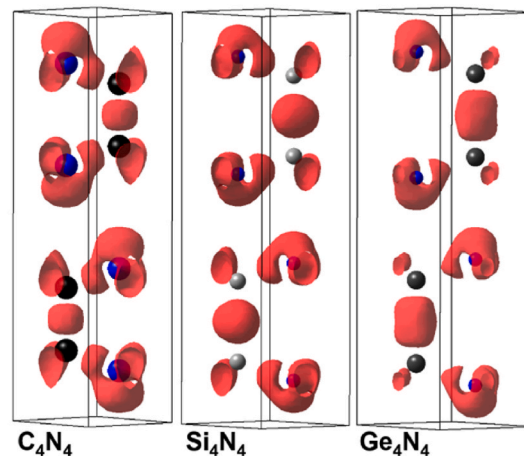
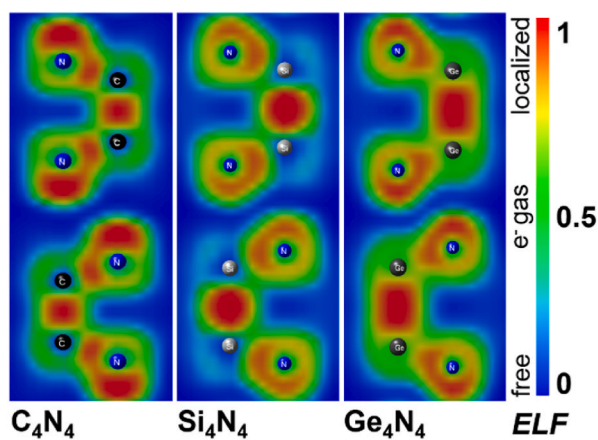


Fig. 5. Electron localization function ELF projected along the long diagonal, *i.e.*, the (110) plane (left). Isosurfaces at $ELF = 0.80$ in red representing domains of localised electrons within the A-A and A-N bonds and respective lone pair of nitrogen atoms (right). (For interpretation of the references to color in this figure legend, the reader is referred to the Web version of this article.)

deviation to expected A_2BX_6 tri-rutile structure [67]. In this context of experimentally characterized and theoretically analysed compounds, proposed A_4N_4 form a structure well aligned with state of research.

The electronic band structures in Fig. 6 point to indirect semi-conducting behaviour with the magnitude of the band gap decreasing across the series from C_4N_4 with 2.412 eV, $\Delta \vec{k} = (0.50 | 0 | 0)$ to Si_4N_4 with 0.698 eV, $\Delta \vec{k} = (0.42 | -0.08 | 0)$ and Ge_4N_4 with 0.217 eV, $\Delta \vec{k} = (-0.08 | 0 | 0)$. For comparison, diamond was calculated with 4.160 eV (experimental value 5.47 eV [68]) and lonsdaleite with 3.279 eV (*cf.* more sophisticated calculations like De et al. [69] with 4.77 eV).

Analysis of the densities of states reveals s-orbitals as first block at low energies (*cf.* appendix Fig. A1). Major contributions to bonding originate from p-orbitals just below the band gap, where nitrogen dominates due to higher electronegativity as compared to that of the respective other constituent (see Fig. 7). The d-orbitals are important for the excited states above the band gap.

2.3. Stability from the mechanical properties and dynamic properties

Analysis of the mechanical behaviour was carried out by calculation of the elastic constants, from which the bulk (*B*) and shear (*G*) moduli were derived. The calculated sets of elastic constants $C_{\alpha\beta}$ are given in Table 2 with all values being positive. C_4N_4 has the largest $C_{\alpha\beta}$ values highlighted by the anisotropic crystal structure underlying smaller magnitudes along the hexagonal *c* directions (C_{33}) versus intra-layer values (C_{11}). The Vickers hardness H_V was calculated from the model of Chen et al. [70] as $H_V = 0.92 \cdot (G/B)^{1.137} \cdot G^{0.708}$. Particularly, C_4N_4 is identified as a super hard material with Vickers hardness $H_V = 32.9$ GPa, while the nitrides of Si and Ge are highly compressible with $H_V = 18.56$ and 10.04 GPa, respectively.

The analysis of the results focused also on Pugh's ratio G_V/B_V allowing to distinguish ductile behavior ($G_V/B_V < 1$) from brittle behavior ($G_V/B_V > 1$) [71]. As a result, with $G_V/B_V = 1.11$ C_4N_4 is more ductile than the other two nitrides, which have G_V/B_V (Si_4N_4) = 1.47, and G_V/B_V (Ge_4N_4) = 1.80. An important criterion of dynamic phase stability is obtained from the phonon dispersions displayed in Fig. 8 along high-symmetry directions of the hexagonal Brillouin zone. The absence of any negative frequencies is indicative of a dynamically stable system for the carbon compound. For Si_4N_4 and Ge_4N_4 residue imaginary acoustic modes (Fig. 8 bottom) indicate that the proposed hexagonal structure would distort, *i.e.* there would be another more stable structure in the energy landscape. Within this study, imaginary modes caused by systematic errors were excluded by employing alternative models for van der Waals interactions, namely state of the art D3+BJ by

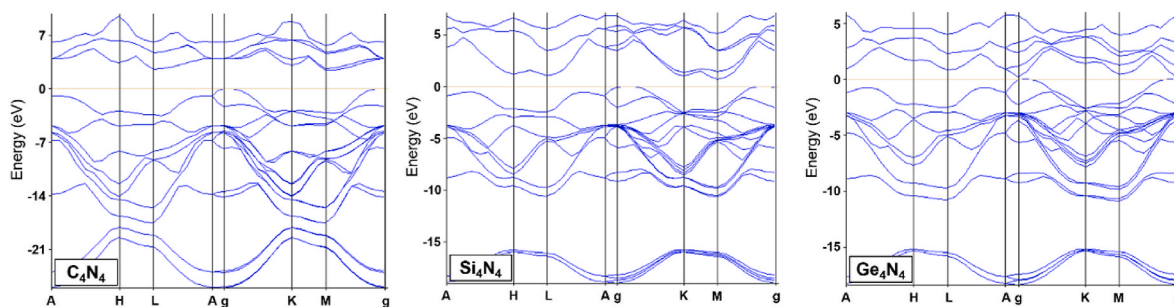


Fig. 6. Electronic band structures. All band gaps are indirect and decrease from C_4N_4 with 2.412 eV, $\Delta \vec{k} = (0.50|0|0)$ over Si_4N_4 with 0.698 eV, $\Delta \vec{k} = (0.42|-0.08|0)$ to Ge_4N_4 with 0.217 eV, $\Delta \vec{k} = (-0.08|0|0)$.

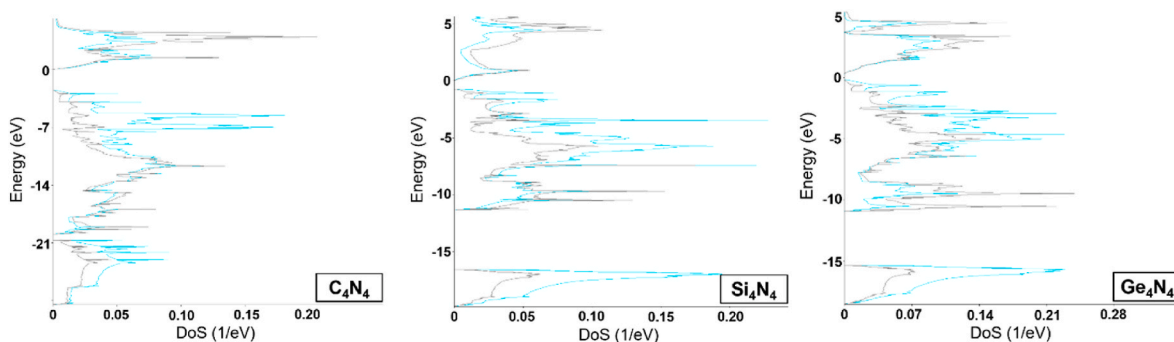


Fig. 7. Densities of states relative to the Fermi level E_F . Contributions of nitrogen atoms shown in cyan and respective Group IV element shown in black. Each compound shows two distinct regions, as the lower part corresponds to the s-states of each constituent separated from the range of p-states where the major bonding occurs. Despite the equal number of atoms of each chemical constituent, the nitrogen states are prevailing in intensity. This is expected from the larger electronegativity on N versus A = C, Si, Ge. Unlike the band structures the band gap decreased from A = C to A = Ge. All three nitrides are considered as semiconducting. (For interpretation of the references to color in this figure legend, the reader is referred to the Web version of this article.)

Table 2

Components of the stiffness matrix in Voigt's notation $C_{\alpha\beta}$, elastic moduli, resulting Pugh's ratio and calculated Vickers hardness. Pugh's Ratio >1.75 indicates ductile behaviour for the germanium compound.

| in GPa: | C_{11} | C_{12} | C_{13} | C_{33} | C_{44} | C_{66} | B | G | E | Γ_{Pugh} | HV |
|-----------|----------|----------|----------|----------|----------|----------|--------|--------|--------|-----------------|-------|
| C_4N_4 | 1143.2 | 148.4 | 9.3 | 223.8 | 69.3 | 497.4 | 316.03 | 283.38 | 654.50 | 1.11 | 44.89 |
| Si_4N_4 | 502.1 | 158.3 | 55.6 | 142.8 | 85.1 | 171.9 | 187.33 | 126.91 | 310.60 | 1.47 | 18.56 |
| Ge_4N_4 | 343.2 | 125.3 | 63.7 | 107.8 | 55.5 | 108.9 | 144.39 | 80.09 | 202.78 | 1.80 | 10.04 |

Grimme with Becke-Johnson damping [72] and optB86b-vdW [73]. Bonds between a large and a small ion like Si-N and Ge-N are known, as covalent bonding occurs even for lead in the form of litharge and masticot PbO. Regarding the optimization algorithm, this change must be of lower symmetry than $P6_3/mnc$ to not be found automatically. This could include super cell effects, where distortions occur on a bigger scale, or local Peilars-like distortion, where a symmetrical A-N-A changes to A-N-A due to anharmonic oscillations of the central atom. Lastly, there could be a double minimum in the energy hyperplane known in ferroelectric compounds. This could be a subject for further analysis in the form of mode-mapping the respective phonon eigenvectors towards lower energies with minimal $P1$ symmetry [74].

While for C_4N_4 the optical modes extend to 38.47 THz similar to observations for diamond by Raman spectroscopy [75], much lower maximum frequencies are observed for the other two nitrides reflecting their smaller elastic constants. Thermodynamic properties were calculated from the phonon frequencies using the statistical thermodynamic approach [76] on a high-precision sampling mesh in the Brillouin zone. Specifically, the temperature dependencies of the heat capacity at constant volume (C_V) and entropy (S) are shown in Fig. 9 in comparison with experimental C_V data for diamond collected by C. V. Raman [77]. It can be observed that the calculated curve for the carbonitride mimics

doubled values of experimental C_V points for diamond regarding slope and curvature. In contrast, the Si and Ge members showed large differences with respect to C_4N_4 regarding C_V relationship with diamond.

2.4. Confirmation of the results with metaGGA calculations

To round off the previous results, additional calculations were performed using two metaGGA functionals, namely, revTPSS and r^2SCAN . The main results in comparison to GGA are shown in Table 3. The metaGGA calculations confirm the proposed unit cells and symmetry, as all deviations in lengths are below 4%. While generally lower total energies are predicted compared to GGA with PBE, it must be noted that this property for Ge_4N_4 is calculated to be 40% higher by revTPSS and 83% lower by r^2SCAN . Still, as the energy of formation of pure germanium follows the same trend and therefore differences are compensated, both metaGGA functionals confirm the range and order of results based on PBE + D2. As discussed in the context of phonon modes, metaGGA was used to show there are no artifacts from GGA causing imaginary modes.

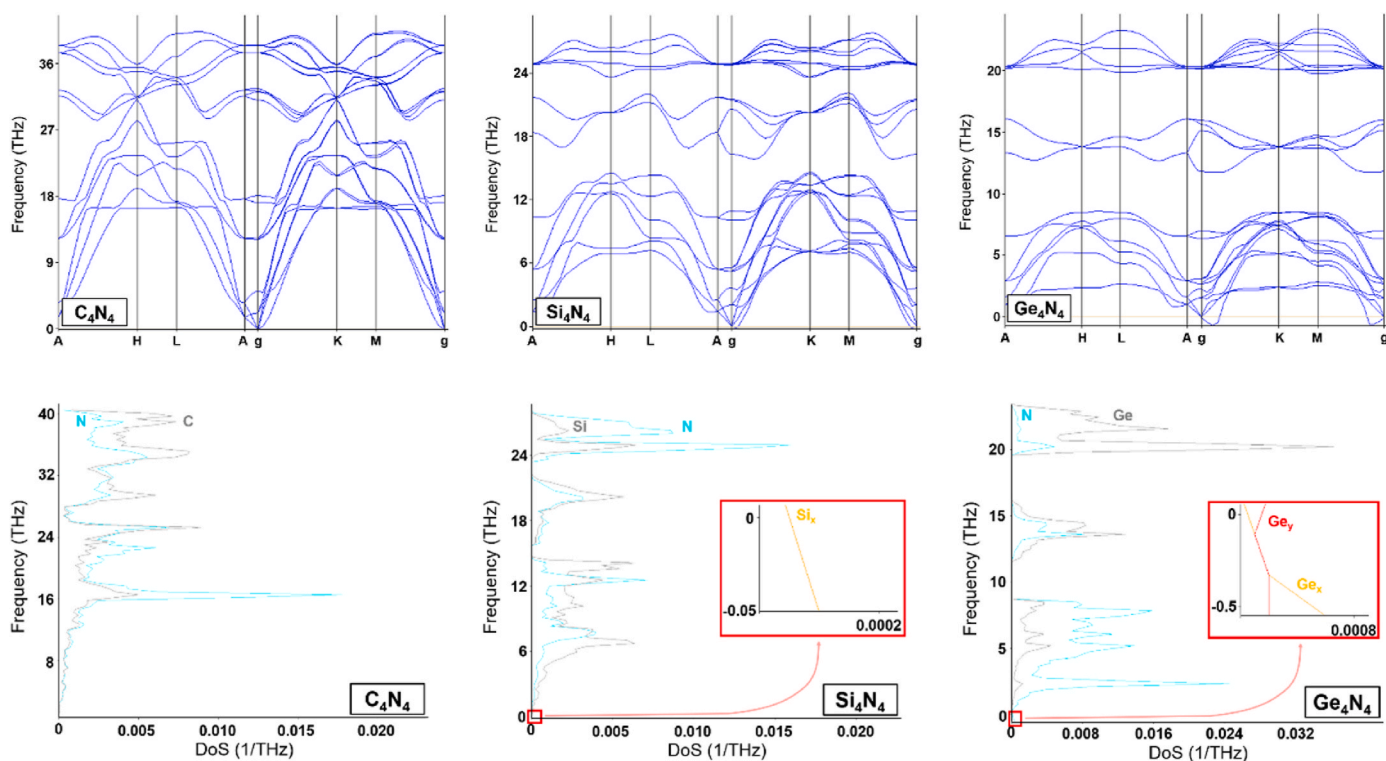


Fig. 8. Phonon dispersion curves within the first Brillouin zone (top) with according density of states by elements. Red inlays show residue imaginary phonon modes for Si in x and for Ge in $x + y$. (For interpretation of the references to color in this figure legend, the reader is referred to the Web version of this article.)

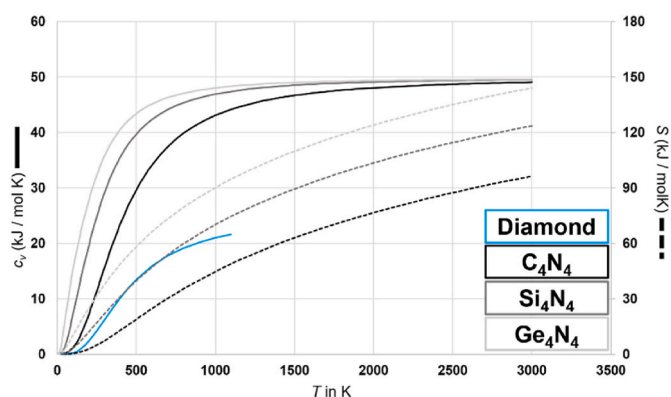


Fig. 9. Specific heat capacities (full line) and entropy component (dashed) as function of temperature. Values compiled from different experimental studies by Raman are given in blue [77]. (For interpretation of the references to color in this figure legend, the reader is referred to the Web version of this article.)

3. Conclusion

In this paper, based on crystal chemistry and DFT calculations, three hexagonal equiatomic nitrides A_4N_4 ($A = C, Si, Ge$) have been proposed, which are characterized by a major role of repulsive N–N lone pairs for the structure made of $\{A_2N_2\}$ bilayers of tetrahedra perpendicular to the hexagonal axis. C_4N_4 was found both mechanically and dynamically stable at ambient conditions. Imaginary phonon modes for Si_4N_4 and Ge_4N_4 signal these systems might tend to distort from the proposed hexagonal structures. Specifically, C_4N_4 was found super-hard with a Vickers hardness of $H_V = 45$ GPa, that decreases along the series due to the increasing volume with atomic radii along the IV^A column leading to rather soft and ductile compounds. The role played by the N($2s^2$) lone pair in structural changes is highlighted with graphical analysis of the

electron localization function. The electronic band structures show a decrease of the semiconducting band gap along the series from C_4N_4 to Ge_4N_4 . Energies of formation suggest high pressure approaches for synthesis of the carbon nitride compound. The present results present a major step towards deeper understanding of these equiatomic nitrides and their role in future applications.

CRediT authorship contribution statement

Samuel D. Griza: Writing – review & editing, Visualization, Validation, Supervision, Software, Project administration, Methodology, Investigation, Conceptualization. **Samir F. Matar:** Writing – review & editing, Writing – original draft, Validation, Methodology, Conceptualization. **Richard Wehrich:** Writing – review & editing, Validation, Conceptualization. **Volker Eyert:** Writing – review & editing, Validation, Software, Methodology, Investigation, Conceptualization.

Data access

The CIFs of relaxed structures and all input parameters of the performed calculations as scripts in the form of *Medea* flowcharts can be provided upon request.

Fundings

S. D. Griza and R. Wehrich gratefully acknowledge prior funding for *Medea* suit and modules by the Bavarian Government (StMWi) in the project K-AXFLUX-H2 (HAM-2109-0044).

Declaration of competing interest

The authors declare that they have no known competing financial interests or personal relationships that could have appeared to influence the work reported in this paper.

Table 3

Comparison of selected results obtained from VASP6 GGA with PBE + D2 and VASP6 metaGGA with revTPSS and r²SCAN.

| C ₄ N ₄ | VASP6 PBE + D2 | VASP6 revTPSS | VASP6 r ² SCAN |
|---|---------------------------------|---------------------------------|---------------------------------|
| a in Å | 2.3634 | 2.3637 | 2.3606 |
| c in Å | 10.5630 | 10.7669 | 10.7451 |
| V_{cell} in Å ³ | 51.10 | 52.10 | 51.86 |
| Shortest distance in Å | 1.455 (C–N) | 1.460 (C–N) | 1.454 (C–N) |
| Atomic position, 4f (2/3, 1/3, z) | z(C) = 0.1732 z(N) = 0.8746 | z(C) = 0.1756 z(N) = 0.8725 | z(C) = 0.1750 z(N) = 0.8721 |
| E_{tot} in eV | –67.88 | –76.54 | –73.10 |
| E_{formation} per UC in eV | +2.44 | +2.94 | +2.64 |
| Si ₄ N ₄ | VASP6 PBE + D2 | VASP6 revTPSS | VASP6 r ² SCAN |
| a in Å | 2.8844 | 2.8760 | 2.8762 |
| c in Å | 12.2023 | 12.5553 | 12.4886 |
| V_{cell} in Å ³ | 87.91 | 89.94 | 89.47 |
| Shortest distance in Å | 1.752 (Si–N) | 1.751 (Si–N) | 1.744 (Si–N) |
| Atomic position, 4f (2/3, 1/3, z) | z(Si) = 0.1521 z(N) = 0.8925 | z(Si) = 0.1545 z(N) = 0.8897 | z(Si) = 0.1538 z(N) = 0.8888 |
| E_{tot} in eV | –62.08 | –71.82 | –78.36 |
| E_{formation} per UC in eV | –6.57 | –6.88 | –7.27 |
| Ge ₄ N ₄ | VASP6 PBE + D2 | VASP6 revTPSS | VASP6 r ² SCAN |
| a in Å | 3.0881 | 3.0725 | 3.0643 |
| c in Å | 12.3956 | 12.7897 | 12.7650 |
| V_{cell} in Å ³ | 102.38 | 104.56 | 103.72 |
| Shortest distance in Å | 1.893 (Ge–N) | 1.894 (Ge–N) | 1.876 (Ge–N) |
| Atomic position, 4f (2/3, 1/3, z) | z(Ge) = 0.1492 z(N) = 0.9022 | z(Ge) = 0.1516 z(N) = 0.9003 | z(Ge) = 0.1514 z(N) = 0.8975 |
| E_{tot} in eV | –51.73 | –29.71 | –91.27 |
| E_{formation} per UC in eV | +0.43 | +8.37 | +0.120 |

Appendix A. Supplementary data

Supplementary data to this article can be found online at <https://doi.org/10.1016/j.jssc.2025.125466>.

Data availability

Data will be made available on request.

References

- Z. Zhao, B. Xu, Y. Tian, Recent advances in superhard materials, *Annu. Rev. Mater. Res.* (2016) 383–406. <https://doi.org/10.1146/annurev-matsci-070115-031649>.
- R.H. Wentorf, R.C. DeVries, F.P. Bundy, Sintered superhard materials, *Science* 208 (1980) 873–880.
- M.L. Cohen, Calculation of bulk moduli of diamond and zinc-blende solids, *Phys. Rev. B* 32 (1985) 7988.
- A.Y. Liu, M.L. Cohen, Prediction of new low compressibility solids, *Science* 245 (1989) 841–842.
- A.Y. Liu, R.M. Wentzcovitch, Stability of carbon nitride solids, *Phys. Rev. B* 50 (1994) 10362.
- D.M. Teter, R.J. Hemley, Low-compressibility carbon nitrides, *Science* 271 (1996) 53–55.
- M. Mattesini, S.F. Matar, Density-functional theory investigation of hardness, stability, and electron-energy-loss spectra of carbon nitrides with C 11 N 4 stoichiometry, *Phys. Rev. B* 65 (2002) 75110.
- V.L. Solozhenko, D. Andrault, G. Fiquet, M. Mezouar, D.C. Rubie, Synthesis of superhard cubic BC 2 N, *Appl. Phys. Lett.* 78 (2001) 1385–1387.
- R. Riedel, A. Greiner, G. Miehe, W. Dressler, H. Fuess, J. Bill, F. Aldinger, The first crystalline solids in the ternary Si-C-N system, *Angew. Chem. Int. Ed. Engl.* 36 (1997) 603–606.
- Y.-L. Li, E. Kroke, A. Klonczynski, R. Riedel, Synthesis of monodisperse spherical silicon dicarbodiimide particles, *Adv. Mater.* 12 (2000) 956–961.
- E. Horvath-Bordon, R. Riedel, P.F. McMillan, P. Kroll, G. Miehe, P.A. van Aken, A. Zerr, P. Hoppe, O. Shebanova, I. McLaren, High-pressure synthesis of crystalline carbon nitride Imide, C₂N₂ (NH), *Angew. Chem.* 119 (2007) 1498–1502.
- A. Salamat, K. Woodhead, P.F. McMillan, R.Q. Cabrera, A. Rahman, D. Adriaens, F. Corà, J.-P. Perrillat, Tetrahedrally bonded dense C 2 N 3 H with a defective wurtzite structure: X-ray diffraction and Raman scattering results at high pressure and ambient conditions, *Phys. Rev. B Condens. Matter* 80 (2009) 104106.
- J.v. Liebig, About some nitrogen compounds, *Ann. Pharm. (Poznan)* 10 (1834) 10.
- W.-J. Ong, L.-L. Tan, Y.H. Ng, S.-T. Yong, S.-P. Chai, Graphitic carbon nitride (g-C₃N₄)-based photocatalysts for artificial photosynthesis and environmental remediation: are we a step closer to achieving sustainability? *Chem. Rev.* 116 (2016) 7159–7329.
- B. Corain, The coordination chemistry of hydrogen cyanide, cyanogen and cyanogen halides, *Coord. Chem. Rev.* 47 (1982) 165–200.
- H. Delbrück, Ueber das Cyan und Paracyan, *J. Prakt. Chem.* 41 (1847) 161–180.
- A.S. Parkes, R.E. Hughes, The crystal structure of cyanogen, *Acta Crystallogr.* 16 (1963) 734–736.
- H. Dong, A.R. Oganov, Q. Zhu, G.-R. Qian, The phase diagram and hardness of carbon nitrides, *Sci. Rep.* 5 (2015) 9870.
- E. Kroke, M. Schwarz, Novel group 14 nitrides, *Coord. Chem. Rev.* 248 (2004) 493–532.
- B. Stavrou, S. Lobanov, H. Dong, A.R. Oganov, V.B. Prakapenka, Z. Konôpková, A. F. Goncharov, Synthesis of ultra-incompressible sp³-hybridized carbon nitride with 1: 1 stoichiometry, *Chem. Mater.* 28 (2016) 6925–6933.
- R.N. Katz, High-temperature structural ceramics, *Science* 208 (1980) 841–847.
- N. Hegedüs, K. Balázi, C. Balázi, Silicon nitride and hydrogenated silicon nitride thin films: a review of fabrication methods and applications, *Materials (Basel)* 14 (2021) 5658.
- R.B. Heimann, Silicon nitride, a close to ideal ceramic material for medical application, *Ceramics* 4 (2021) 208–223.
- S.J. Wang, J.W. Chai, J.S. Pan, A.C. Huan, Thermal stability and band alignments for Ge₃N₄ dielectrics on Ge, *Appl. Phys. Lett.* 89 (2006).
- M.P. Shemkunas, W.T. Petuskey, A.V. Chizmeshya, K. Leinenweber, G.H. Wolf, Hardness, elasticity, and fracture toughness of polycrystalline spinel germanium nitride and tin nitride, *J. Mater. Res.* 19 (2004) 1392–1399.
- R. Wehrich, V. Eyert, S.F. Matar, Structure and electronic properties of new model dinitride systems: a density-functional study of CN₂, SiN₂, and GeN₂, *Chem. Phys. Lett.* 373 (2003) 636–641.
- K. Niwa, H. Ogasawara, M. Hasegawa, Pyrite form of group-14 element pernitrides synthesized at high pressure and high temperature, *Dalton Trans.* (2003) 46 (2017) 9750–9754.
- P.L. Jurzick, G. Krach, L. Brüning, W. Schnick, M. Bykov, Synthesis and crystal structure of silicon pernitride SiN₂ at 140 GPa, *Acta Crystallogr. E: Crystallograph. Commun.* 79 (2023).
- P. Hohenberg, W. Kohn, Inhomogeneous electron gas, *Phys. Rev.* 136 (1964) B864.
- W. Kohn, L.J. Sham, Self-consistent equations including exchange and correlation effects, *Phys. Rev.* 140 (1965) A1133.
- G. Kresse, J. Furthmüller, Efficient iterative schemes for ab initio total-energy calculations using a plane-wave basis set, *Phys. Rev. B* 54 (1996) 11169.
- G. Kresse, D. Joubert, From ultrasoft pseudopotentials to the projector augmented-wave method, *Phys. Rev. B* 59 (1999) 1758.
- P.E. Blöchl, Projector augmented-wave method, *Phys. Rev. B* 50 (1994) 17953.
- J.P. Perdew, K. Burke, M. Ernzerhof, Generalized gradient approximation made simple, *Phys. Rev. Lett.* 77 (1996) 3865.
- S. Grimme, Accurate description of van der Waals complexes by density functional theory including empirical corrections, *J. Comput. Chem.* 25 (2004) 1463–1473.
- P.E. Blöchl, O. Jepsen, O.K. Andersen, Improved tetrahedron method for Brillouin-zone integrations, *Phys. Rev. B* 49 (1994) 16223.
- H.J. Monkhorst, J.D. Pack, Special points for Brillouin-zone integrations, *Phys. Rev. B* 13 (1976) 5188.
- R.F.W. Bader, A quantum theory of molecular structure and its applications, *Chem. Rev.* 91 (1991) 893–928.
- A.D. Becke, K.E. Edgecombe, A simple measure of electron localization in atomic and molecular systems, *J. Chem. Phys.* 92 (1990) 5397–5403.
- Y. Le Page, P. Saxe, Symmetry-general least-squares extraction of elastic coefficients from ab initio total energy calculations, *Phys. Rev. B* 63 (2001) 174103.
- Y. Le Page, P. Saxe, Symmetry-general least-squares extraction of elastic data for strained materials from ab initio calculations of stress, *Phys. Rev. B* 65 (2002) 104104.
- A. Togo, I. Tanaka, First principles phonon calculations in materials science, *Scr. Mater.* 108 (2015) 1–5.
- K. Parlinski, Z.Q. Li, Y. Kawazoe, First-principles determination of the soft mode in cubic ZnO 2, *Phys. Rev. Lett.* 78 (1997) 4063.
- A.P. Shevchenko, A.A. Shabalina, I.Y. Karpukhin, V.A. Blatov, Topological representations of crystal structures: generation, analysis and implementation in the TopCryst system, *Sci. Technol. Adv. Mater.: Methods* 2 (2022) 250–265.
- G.I. Finch, H. Wilman, The diffraction of electrons by graphite, *Proc. Roy. Soc. Lond. Math. Phys. Sci.* 155 (1936) 345–365.
- S.I. Uspenskaya, N.A. Kolchomanov, A.A. Eliseev, S.V. Krynina, Investigation into physicochemical properties of alloyed synthetic diamonds, *Zhurnal Neorganicheskoi Khimii* 24 (1979) 7–11.
- M.E. Straumanis, E.Z. Aka, Lattice parameters, coefficients of thermal expansion, and atomic weights of purest silicon and germanium, *J. Appl. Phys.* 23 (1952) 330–334.

- [48] T. Soma, H. Iwanami, H. Matsuo, Phase transition under pressure of Si-Ge solid solutions, *Solid State Commun.* 42 (1982) 469–471.
- [49] R.J. Needs, R.M. Martin, Transition from β -tin to simple hexagonal silicon under pressure, *Phys. Rev. B* 30 (1984) 5390.
- [50] J.Z. Hu, L.D. Merkle, C.S. Menoni, L.L. Spain, Crystal data for high-pressure phases of silicon, *Phys. Rev. B* 34 (1986) 4679.
- [51] S.J. Duclos, Y.K. Vohra, A.L. Ruoff, Hcp to fcc transition in silicon at 78 GPa and studies to 100 GPa, *Phys. Rev. Lett.* 58 (1987) 775.
- [52] C. Li, C. Wang, J. Han, L. Yan, B. Deng, X. Liu, A comprehensive study of the high-pressure–temperature phase diagram of silicon, *J. Mater. Sci.* 53 (2018) 7475–7485.
- [53] P. Duwez, R.H. Willens, W. Klement Jr., Metastable solid solutions in the gallium antimonide-germanium pseudobinary system, *J. Appl. Phys.* 31 (1960) 1500.
- [54] G.A. Voronin, C. Pantea, T.W. Zerda, J. Zhang, L. Wang, Y. Zhao, In situ X-ray diffraction study of germanium at pressures up to 11 GPa and temperatures up to 950 K, *J. Phys. Chem. Solid.* 64 (2003) 2113–2119.
- [55] T.A. Scott, Solid and liquid nitrogen, *Phys. Rep.* 27 (1976) 89–157.
- [56] J.A. Venables, C.A. English, Electron diffraction and the structure of α -N₂, *Acta Crystallogr. B Struct. Crystallogr. Cryst. Chem.* 30 (1974) 929–935.
- [57] J. Tao, J.P. Perdew, V.N. Staroverov, G.E. Scuseria, Climbing the density functional ladder: Nonempirical meta-generalized gradient approximation designed for molecules and solids, *Phys. Rev. Lett.* 91 (2003) 146401.
- [58] J.P. Perdew, A. Ruzsinszky, G.I. Csonka, L.A. Constantin, J. Sun, Workhorse semilocal density functional for condensed matter physics and quantum chemistry, *Phys. Rev. Lett.* 103 (2009) 26403.
- [59] J.W. Furness, A.D. Kaplan, J. Ning, J.P. Perdew, J. Sun, Accurate and numerically efficient r2SCAN meta-generalized gradient approximation, *J. Phys. Chem. Lett.* 11 (2020) 8208–8215.
- [60] J.P. Perdew, K. Schmidt (Eds.), *Jacob's Ladder of Density Functional Approximations for the Exchange-Correlation Energy*, American Institute of Physics, 2001.
- [61] A. Kuhn, A. Chevy, R. Chevalier, Refinement of the 2H GaS β -type, *Acta Crystallogr. B Struct. Crystallogr. Cryst. Chem.* 32 (1976) 983–984.
- [62] F. Hergert, S. Jost, R. Hock, M. Purwins, A crystallographic description of experimentally identified formation reactions of Cu (In, Ga) Se₂, *J. Solid State Chem.* 179 (2006) 2394–2415.
- [63] J. von Appen, M.-W. Lumey, R. Dronskowski, Mysterious platinum nitride, *Angew. Chem. Int. Ed.* 45 (2006) 4365–4368.
- [64] T. Nilges, P. Schmidt, R. Wehrich, Phosphorus: the Allotropes, Stability, Synthesis, and Selected Applications, *Encyclopedia of Inorganic and Bioinorganic Chemistry*, 2011, pp. 1–18.
- [65] J. Galy, S.F. Matar, Electron Lone-Pairs Stereochemistry and Drastic van der Waals and Pressure Effects in AsF₃ from First Principles, *Condens. Matter* 6 (2021) 31.
- [66] R. Enjalbert, J. Galy, STRUCTURE CRISTALLINE DU TRIFLUORURE D'ARSENIC ASF₃ A 193 K, 1979.
- [67] S.F. Matar, Se₂TiO₆E₂ ternary oxide characteristic of isolated TiO₆ octahedra with the shear effect of SeIVe electron lone pair (E): combined crystal chemistry and ab initio study, *J. Phys. Chem. C* 124 (2020) 12281–12285.
- [68] H. Yang, Y. Ma, Y. Dai, Progress of structural and electronic properties of diamond: a mini review, *Functional Diamond* 1 (2022) 150–159.
- [69] A. De, C.E. Pryor, Electronic structure and optical properties of Si, Ge and diamond in the lonsdaleite phase, *J. Phys. Condens. Matter* 26 (2014) 45801.
- [70] X.-Q. Chen, H. Niu, D. Li, Y. Li, Modeling hardness of polycrystalline materials and bulk metallic glasses, *Intermetallics* 19 (2011) 1275–1281.
- [71] O.N. Senkov, D.B. Miracle, Generalization of intrinsic ductile-to-brittle criteria by Pugh and Pettifor for materials with a cubic crystal structure, *Sci. Rep.* 11 (2021) 4531.
- [72] S. Grimme, S. Ehrlich, L. Goerigk, Effect of the damping function in dispersion corrected density functional theory, *J. Comput. Chem.* 32 (2011) 1456–1465.
- [73] J. Klimeš, D.R. Bowler, A. Michaelides, Van der Waals density functionals applied to solids, *Phys. Rev. B Condens. Matter* 83 (2011) 195131.
- [74] I. Pallikara, P. Kayastha, J.M. Skelton, L.D. Whalley, The physical significance of imaginary phonon modes in crystals, *Electron. Struct.* 4 (2022) 33002.
- [75] R.S. Krishnan, Raman spectrum of diamond, *Nature* 155 (1945) 171.
- [76] M.T. Dove, *Introduction to Lattice Dynamics*, Cambridge university press, 1993.
- [77] C.V. Raman (Ed.), *The Heat Capacity of Diamond between 0 and 1000° K*, Springer, 1957.